

# Analysis of Trabecular Bone Structure with Multidetector Spiral Computed Tomography in a Simulated Soft-Tissue Environment

Jan S. Bauer · Thomas M. Link · Andrew Burghardt ·  
Tobias D. Henning · Dirk Mueller · Sharmila Majumdar ·  
Sven Prevrhal

Received: 28 August 2006 / Accepted: 27 February 2007 / Published online: 23 May 2007  
© Springer Science+Business Media, LLC 2007

**Abstract** We investigated the influence of soft tissue (ST) on image quality by high-resolution multidetector computed tomography (MDCT) scans and assessed the effect of surrounding ST on the quantification of trabecular bone structure. Eight bone cores obtained from human proximal femoral heads discarded during hip replacement surgery were scanned with micro-computed

tomography ( $\mu$ CT) as well as with MDCT both without (w/o) and with (w) simulated surrounding ST, where a phantom imitated a human torso. Signal-to-noise ratio (SNR) and contrast-to-noise ratio (CNR) were measured in all scans. Apparent trabecular bone structure parameters were calculated and compared to similar parameters obtained in coregistered sections of the  $\mu$ CT scans. Residual errors were calculated as root-mean-square (RMS) errors relative to the  $\mu$ CT measurements. Compared to  $\mu$ CT results, trabecular structure parameters were overestimated by MDCT both w and w/o ST. SNR and CNR were significantly higher in the scans w/o ST. Significant correlations between  $\mu$ CT and MDCT results were found for bone fraction ( $r = 0.90$  w/o ST,  $r = 0.84$  w ST), trabecular number, and separation. RMS ranged from 10% to 15% for MDCT w/o ST and from 10% to 17% for MDCT w ST. Only bone fraction showed significantly different RMS and correlations for scans w/o vs. w ST ( $P < 0.05$ ). This study showed that MDCT is able to visualize trabecular bone structure in an *in vivo*-like setting at skeletal sites within the torso such as the proximal femur. Even though ST scatter compromises image quality substantially, the major characteristics of the trabecular network can still be appreciated and quantified.

**Funding source** Seed grant by the Department of Radiology, University of California, San Francisco, CA, USA

J. S. Bauer · T. M. Link · A. Burghardt · T. D. Henning ·  
S. Majumdar · S. Prevrhal  
Musculoskeletal and Quantitative Imaging Research,  
Department of Radiology, University of California in San  
Francisco, San Francisco, CA, USA  
e-mail: jsb@roe.med.tum.de

T. M. Link  
e-mail: Thomas.Link@radiology.ucsf.edu

A. Burghardt  
e-mail: andrew.burghardt@radiology.ucsf.edu

T. D. Henning  
e-mail: tobias.henning@radiology.ucsf.edu

S. Majumdar  
e-mail: sharmila.majumdar@radiology.ucsf.edu

S. Prevrhal  
e-mail: sven.prevrhal@radiology.ucsf.edu

J. S. Bauer (✉) · D. Mueller  
Department of Radiology, Klinikum rechts der Isar, Technische  
Universität München, Ismaninger Str. 22, Munich 81675,  
Germany  
e-mail: jsb@roe.med.tum.de

D. Mueller  
e-mail: dirk.mueller@gmx.de

**Keywords** Trabecular bone microarchitecture ·  
Bone structure analysis · Micro-computed tomography ·  
Multidetector row computed tomography · Osteoporosis ·  
Femur · Scattering artifact

## Introduction

Osteoporosis represents a major health problem, causing more than 2 million fractures per year in the United States

with a burden of \$19 billion to the health-care systems in 2005 [1, 2]. On the microscopic level, bone is subject to a constant remodeling or turnover process to adapt to mechanical challenges or replace overly aged tissue, consisting of bone resorption and subsequent formation. In osteoporosis, higher net loss of bone at the remodeling site then leads to deeper resorption lacunae, penetration and even removal of whole trabeculae, and ultimately compromised mechanical integrity. Prominent features of increased bone turnover and resorption are therefore an increase in trabecular separation (Tb.Sp) and decreases in bone volume fraction (BV/TV), trabecular number (Tb.N), and trabecular thickness (Tb.Th).

With the development of multidetector spiral computed tomography (MDCT), spatial resolutions as well as imaging speed have improved substantially, and in-plane spatial resolutions of down to 300  $\mu\text{m}$  are now clinically achievable. This is close to the size and spacing of single trabeculae (50–200  $\mu\text{m}$  and 1,000–2,000  $\mu\text{m}$ , respectively). In an experimental setting, micro-computed tomography ( $\mu\text{CT}$ ) provides even higher spatial resolution, usually below 50  $\mu\text{m}$  (synchrotron-based devices provide less than 1  $\mu\text{m}$ ), and is therefore able to display the true three-dimensional (3D) trabecular structure in bone specimens *ex vivo* [3].

Several studies have shown that the spatial resolution of MDCT is poorer than required for measuring the size of individual trabeculae but potentially sufficient for assessing trabecular spacing and different texture properties of the trabecular network [4–8]. These studies were able to improve the assessment of bone strength with such structural measurements [4–8]. However, most of these studies have either been performed at peripheral skeletal sites or used bone samples without surrounding soft tissue (ST). None of these studies has examined the effect of surrounding ST on image quality and the ability to display trabecular structure, which can be quite substantial. Since beam hardening and noise characteristics are strongly influenced by the size and composition of the whole scanned cross section and the trabecular dimensions are at the spatial resolution limit of current CT technology, a ST environment is expected to reduce contrast, CT value homogeneity, and spatial resolution. The effect on the quantification of trabecular structure is yet unknown.

The aim of this study was therefore (1) to acquire MDCT images of trabecular bone without (w/o) and with (w) simulation of the ST environment to be expected *in vivo* and (2) to analyze the ST effect on structural parameters, analogous to standard histomorphometry, using  $\mu\text{CT}$  measurements as a standard of reference.

## Materials and Methods

### Specimens

Four femoral heads were obtained from patients who underwent total hip replacement surgery due to advanced osteoarthritis. The study was performed in line with legislative and institutional guidelines for human research. Two cylindrical specimens with a diameter of 0.8 cm and a length of 2.5 cm were harvested from each of the four femoral heads. The specimens were placed in sealed and labeled plastic tubes filled with saline solution and degassed prior to MDCT for at least 24 hours. Between the imaging procedures, the specimens were stored at  $-80^{\circ}\text{C}$ ; before scanning, each specimen was allowed to thaw to room temperature for about 18 hours.

### $\mu\text{CT}$

Using X-ray-based  $\mu\text{CT}$ , 3D bone structure of whole anatomic specimens can be measured nondestructively in a reliable way [9]. High correlations between conventional histomorphometric and 2D  $\mu\text{CT}$  analysis have been found, and the method has been established as a standard of reference for the study of bone architecture [3, 10].  $\mu\text{CT}$  was carried out on a Scanco (Bassersdorf, Switzerland)  $\mu\text{CT}40$ . A spatial resolution with a voxel size of  $8 \times 8 \times 8 \mu\text{m}$  was obtained, and the imaging time was approximately 4 hours/specimen. Trabecular bone structure calculations from these data sets were used as the gold standard for comparison with those derived from MDCT.

### MDCT

Axial MDCT images of the femur specimens were obtained with a standard 16-row MDCT (MX-8000; Philips Medical, Cleveland, OH). Specimens were positioned on a CT Calibration Phantom (Mindways Software, Austin, TX), which was used as a CT number reference standard. The phantom contained five rod-shaped inserts of solid reference materials calibrated against  $\text{K}_2\text{HPO}_4$ /water solutions that allowed for conversion of CT Hounsfield units to  $\text{K}_2\text{HPO}_4$ -equivalent bone mineral density (BMD) values.

Two scan protocols were employed: w and w/o surrounding ST. The scans w/o ST simulation were performed by placing the small water-filled plastic tubes containing the specimens directly on the phantom. The tube current was 120 kVp with 300 mAs/slice and a scan time of about 12 seconds/bone sample. A slice thickness of 0.8 mm was chosen with an increment of 0.4 mm and a collimation of

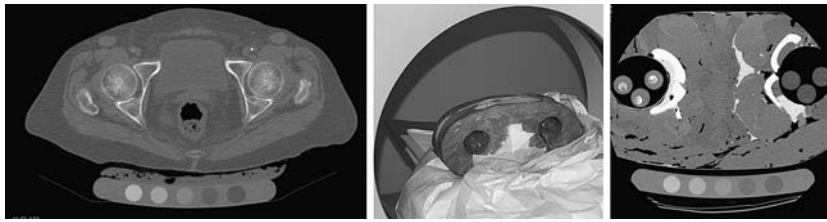


**Fig. 1** One of the CT slides (*left*) of the hip that were used as a reference to build the phantom (*middle*). On the *right* is a representative section of three specimens inside the phantom. Note

that the outer parts of the phantom are not visualized in this section due to the limited circular reconstruction in high-resolution scan mode

16 x 0.75 mm. Images were reconstructed with a high-resolution “D” kernel at a very small field of view of 11.1 cm and a standard image matrix size of 512 x 512 pixel, yielding an in-plane spatial resolution of 0.35 mm (50% point spread function).

For the ST simulation, the specimens were placed in an oval, special-purpose phantom, made of porcine muscles, fat, and bone, equal to an average 75 kg person at the hip. The design of the phantom was based on the evaluation of several *in vivo* CT scans of patients at our institution (Fig. 1). The scan protocol was similar to the one used in the scans w/o ST. Just a larger field of view of 17.8 cm had to be used, to cover both bone sample and calibration phantom in one image. However, the spatial resolution remained similar compared to the scans w/o ST as the limiting factor for the spatial resolution was the modulation transfer function. The modulation transfer function is dependent on the radiation dose as well as the kernel used, which were similar in both scan protocols.

### Image Analysis

To perform the image analysis, the  $\mu$ CT and MDCT data were transferred to a workstation equipped with software developed in-house using IDL (Interactive Display Language 6.0; ITT Visual Information Solutions, Boulder, CO, USA). In a first step, image data sets were visually co-registered. All regions available in the three image data sets were used for further evaluation. To compare image quality, signal-to-noise ratio (SNR) and contrast-to-noise ratio (CNR) were calculated for every specimen and image modality. In case of MDCT, SNR was defined as the mean signal intensity of the bone specimen divided by the standard deviation of the background (air). In case of  $\mu$ CT, SNR was defined as the signal intensity of bone divided by the standard deviation of the background. The CNR was calculated as the mean signal intensity of the bone minus the mean signal intensity of the marrow space divided by the standard deviation of the background. The CT signal homogeneity (CTSH) was defined as the mean signal intensity of water divided by the standard deviation of water.

For quantitative evaluation of trabecular bone structure, all images were binarized by absolute thresholding to bone (“on” pixels) and marrow (“off” pixels). We applied a global threshold to all images, which was optimized visually prior to all analysis procedures as described by other researchers [6, 7, 11]. The aim of this optimization was to match the structure revealed by MDCT in the binarized images with the visual impression in the gray-scale images. Due to partial volume effects, care has to be taken that specimens with dense trabecular bone structure do not only consist of “on” pixels and osteoporotic specimens still show trabecular structure, thus not only “off” pixels. This threshold was determined to be 157 g/cm<sup>3</sup> hydroxyapatite in case of the MDCT images w/o ST and 108 g/cm<sup>3</sup> hydroxyapatite in case of the MDCT images w ST. This hydroxyapatite threshold was reconverted to Hounsfield units for every image using the CT calibration phantom. In the  $\mu$ CT images, where no phantom was used, the best threshold was chosen based on the bimodal histogram. It was determined to be 8,000 in the  $\mu$ CT-specific gray-value distribution. After binarization of the images with this threshold, a circular region of interest (ROI) with a diameter of 6 mm was selected for every slice in the center of the specimen.

Four morphological parameters analogous to standard bone histomorphometry were calculated within these ROIs. The current standard of image processing to calculate these parameters is 3D distance transformation. However, as the slice thickness of the MDCT images was substantially higher than the in-plane spatial resolution, parameters could not be calculated using this simple method. Therefore we used a plate-rod model proposed by Parfitt et al. [12], which considers the different spatial resolutions and assumes a plate-like bone structure [see also 13]. The underlying computations were based on the mean intercept length method [14]. For reasons of comparability, the same method was used for the  $\mu$ CT data sets. This analysis was performed with software built in-house using an IDL interface [12, 15]. Parameters were calculated for every single slice and then averaged for 1.2-mm-thick sections containing three MDCT slices and the corresponding 150  $\mu$ CT slices. The morphological parameters assessed in

**Fig. 2** Representative, corresponding section from specimen 7 obtained by  $\mu$ CT (left), CT w/o ST (middle), and CT w ST simulation (right). Upper row represents unprocessed image data; lower row represents thresholded images. Note the scattering artifacts in the CT image w ST that compromise image quality; however, the major trabecular characteristics are still visible

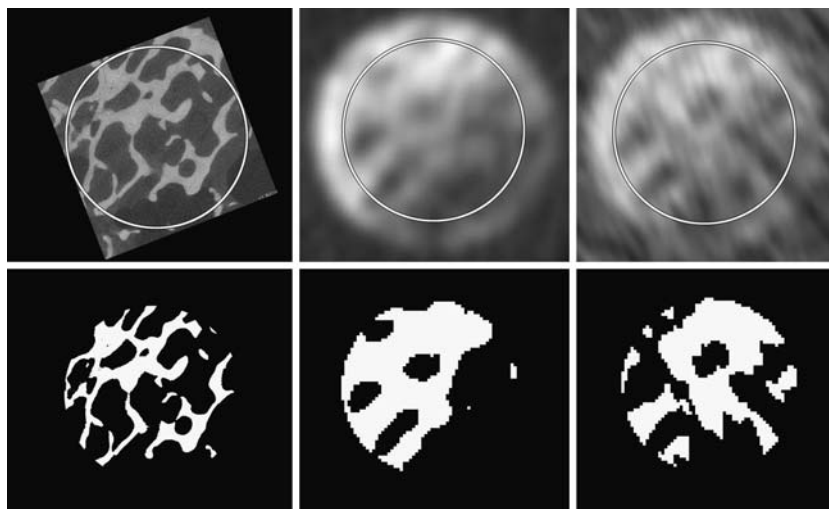


**Table 1** Major image characteristics for the different scan protocols (SNR, CNR, CTSH)

	$\mu$ CT	MDCT	MDCT <sub>soft tissue</sub>
Spatial resolution in plane (mm)	0.008	0.35	0.35
Slice thickness (mm)	0.008	0.8	0.8
SNR		437	54.3
CNR		138	16.8
CTSH (%)		110	20.4

**Table 2** Mean values and standard deviations of the structural parameters of the eight bone specimens: relative difference factor compared to  $\mu$ CT-derived parameters (in parentheses)

	$\mu$ CT	MDCT	MDCT <sub>soft tissue</sub>
BV/TV	0.19 ± 0.06	0.28 ± 0.15 (1.5)	0.39 ± 0.12 (2.0)
Tb.N (1/mm)	1.79 ± 0.34	0.34 ± 0.10 (0.2)	0.37 ± 0.07 (0.2)
Tb.Sp (mm)	0.48 ± 0.11	2.26 ± 0.83 (4.7)	2.88 ± 1.15 (6.0)
Tb.Th (mm)	0.15 ± 0.01	0.83 ± 0.40 (5.7)	0.89 ± 0.37 (6.1)

this study were BV/TV (bone volume/total volume), Tb.Th, Tb.N, and Tb.Sp. They were labeled apparent (app.) as a model was used for the calculation [16].

**Statistical Analysis**

Mean and standard deviation were calculated for all 1.2 mm sections. The MDCT-derived parameters w and w/o ST were correlated with the  $\mu$ CT parameters. The resulting correlation coefficients were compared using Fisher’s Z-transform to evaluate significant differences. Residual errors of the predicted MDCT measurements were calculated as root-mean-square (RMS) errors, in absolute values and as a percentage of the mean  $\mu$ CT measurements. RMS

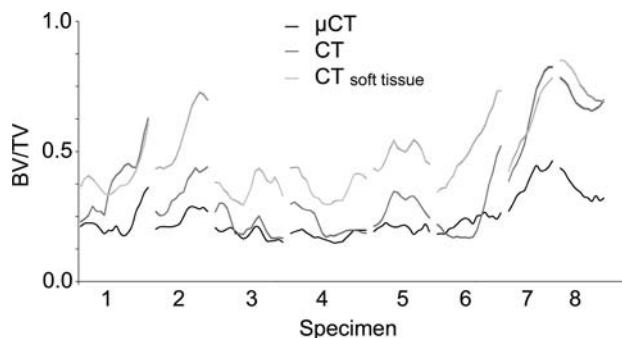


**Fig. 3** BV/TV for all 126 evaluated sections in the eight specimens for the  $\mu$ CT (black), CT (dark gray), and CT w ST simulation (light gray)

differences were tested for significance using analysis of variance. The threshold for significance was  $P < 0.05$  for the whole study. All statistical computations were processed using JMP 5.1 (SAS Institute, Cary, NC) and SPSS (Chicago, IL) 11.5 software.

**Results**

In the eight analyzed specimens, 126 corresponding 1.2-mm-thick sections were compared among the different imaging modalities (Fig. 2). SNR was highest in the MDCT images w/o ST (437, Table 1). It was eight times lower in the MDCT images w ST (54.3) and lowest in the  $\mu$ CT data (15.1). A similar trend was found for CNR (Table 1). The signal homogeneity was five times higher w/o ST compared to the scans w ST. The differences can be appreciated in Figure 2.

As revealed by  $\mu$ CT, average app. BV/TV of all samples was 0.19 (Table 2). There was a substantial variation

**Table 3** Correlation coefficients of the 126 evaluated sections of the eight specimens between  $\mu$ CT and CT w and w/o surrounding ST

<i>r</i> (Pearson)	$\mu$ CT vs. MDCT	$\mu$ CT vs. MDCT <sub>soft tissue</sub>	MDCT vs. MDCT <sub>soft tissue</sub>
BV/TV*	0.90	0.84	0.83
Tb.N	0.76	0.71	0.70
Tb.Sp	0.76	0.72	0.85
Tb.Th	n.s.	n.s.	0.82

\*Differences in correlation coefficients between CT w and w/o surrounding ST were significant only for BV/TV ( $P < 0.05$ ). n.s., not significant

**Table 4** Residual errors, calculated as RMS errors of the 126 evaluated sections in the eight specimens between  $\mu$ CT and CT w and w/o surrounding ST

RMS error	$\mu$ CT vs. MDCT	$\mu$ CT vs. MDCT <sub>soft tissue</sub>
BV/TV*	0.03 (13%)	0.03 (17%)
Tb.N (1/mm)	0.22 (12%)	0.23 (13%)
Tb.Sp (mm)	0.07 (15%)	0.08 (16%)
Tb.Th (mm)	0.01 (10%)	0.01 (10%)

Relative errors are shown in parentheses. \*Differences in RMS errors between CT w and w/o surrounding ST were significant only for BV/TV ( $P < 0.05$ )

throughout the sections, with a minimum of 0.06 and a maximum of 0.37 (Fig. 3). This variation corresponded to the location of the harvest site: the trabecular structure was denser in the central region of the femoral heads compared to the periphery. Comparing MDCT and  $\mu$ CT, app. BV/TV was overestimated by MDCT by a factor of 1.5 w/o ST and by a factor of 2.0 w surrounding ST (Table 2). Average app. Tb.N was 1.8/mm as measured by  $\mu$ CT and was underestimated by a factor of 5 by MDCT independent of ST presence. Average app. Tb.Sp was 0.5 mm in the  $\mu$ CT scans and overestimated by MDCT by a factor of 4.7 w/o ST and by a factor of 6.0 w surrounding ST. Apparent Tb.Th was 5.7 times higher in the MDCT scans w/o ST and 6.1 times higher in the MDCT scans w surrounding ST compared to 0.15 mm in the  $\mu$ CT scans. This was the largest relative difference between the  $\mu$ CT and MDCT scans (Figs. 2 and 3).

Although the relative differences between parameters obtained with  $\mu$ CT and MDCT were quite substantial, significant correlations were found between the different methods. MDCT showed the highest correlation with  $\mu$ CT in case of app. BV/TV w/o ST (Table 3,  $r = 0.90$ ). This was significantly higher compared to MDCT w ST ( $P < 0.05$ ,  $r = 0.84$ ). Lower but still significant correlation coefficients were found for the parameters app. Tb.N and app. Tb.Sp (both  $r = 0.76$  w/o ST;  $r = 0.71$  and  $r = 0.72$ , respectively, w ST). For these parameters, the difference between scans

w and w/o ST was not significant ( $P > 0.05$ ). No significant correlation was found between  $\mu$ CT and MDCT for app. Tb.Th for both scans w and w/o ST.

The RMS of the residual errors for MDCT are shown in Table 4. In case of BV/TV, they were 13% in the scans w/o ST and 17% in the scans w ST. This was the only parameter showing a significant difference for MDCT w ST as opposed to w/o ST. The RMS for the other parameters ranged from 10% to 15% for MDCT w/o ST and from 10% to 16% for MDCT w ST.

Comparing MDCT w and w/o ST, significant correlations were found for all parameters, ranging from  $r = 0.85$  for app. Tb.Sp to  $r = 0.70$  for app. Tb.N (app. BV/TV  $r = 0.83$ , app. Tb.Th  $r = 0.82$ ; all  $P < 0.05$ ).

## Discussion

In this study, we investigated the feasibility of trabecular structure assessment with multirow-detector whole-body CT. Although similar studies have been reported, this is the first to our knowledge to investigate the feasibility of structural measurements in a simulated *in vivo* scenario at the proximal femur by including ST with associated loss of spatial resolution and image contrast. The significant, robust correlations of trabecular architectural parameters with  $\mu$ CT as the standard of reference indicate that MDCT is able to reveal trabecular structure patterns *in vivo*, even at skeletal sites within the torso such as the proximal femur. Even though scattering artifacts compromise visual image quality substantially, the major characteristics of the trabecular network still can be visualized and quantified.

The introduction of multirow solid-state detector technology in whole-body CT has recently improved CT performance characteristics considerably [17, 18]. MDCT scanners are providing much faster volume coverage. Ultrahigh-resolution modes have vastly improved spatial resolution, achieving near-isotropic in-plane and cross-plane spatial resolutions of down to 300  $\mu$ m, making MDCT clearly superior to standard CT for analyzing trabecular bone structure [5].

However, beam hardening and noise characteristics are strongly influenced by the size and composition of the whole scanned cross section. SNR and CNR decreased about eightfold in the scans w ST in this study. The scattering artifacts can clearly be appreciated in the presented images. Efforts are under way to reduce these artifacts, but problems remain in high-resolution imaging with limited radiation dose [19–21]. At the same time, new CT systems are being developed to further improve spatial resolution [22].

Prior studies showed that high-resolution MDCT is useful for evaluating trabecular structure in different ana-



otic regions of the body [4, 5, 23, 24]. Cortet et al. [24] showed that structural parameters of trabecular bone (app. BV/TV, app. Tb.N, app. Tb.Sp) as determined from CT images of the calcaneus correlate strongly with those determined using histomorphometry under *in vitro* conditions. Link et al. [4] found that structural parameters determined in MDCT images of the distal radius may be used to determine trabecular bone structure. Patel et al. [7] calculated structural parameters from MDCT images of the calcaneus acquired with four different protocols. Using high-dose, high-resolution protocols, donors with and without osteoporotic vertebral fractures could be differentiated best. All these studies were performed at peripheral skeletal sites.

Comparing different skeletal sites, weak correlations were found for bone strength as well as for BMD [25, 26]. Thus, fracture risk should be determined at the site of interest. In osteoporosis, clinically the most severe fractures occur at skeletal sites within the torso, such as the spine and the proximal femur [27, 28]. Several studies have analyzed the trabecular structure of the central skeleton and the proximal femur [5, 6, 8, 23, 29, 30]. Gordon et al. [23] found that assessment of vertebral trabecular structure from high-resolution CT images is useful in discriminating subjects with vertebral fractures and potentially useful for predicting future fractures *in vivo*. Bauer et al. [5] calculated structural parameters of vertebral specimens using MDCT images. They found significant correlations with structural measurements of  $\mu$ CT. Correlations with biomechanical strength were significantly higher for structural parameters than for BMD in that study. Although all these studies showed the ability of MDCT to depict trabecular bone structure, only one study used scans with surrounding ST at the thoracic spine: Ito et al. [6] performed *in vivo* scans of the thoracic spine in 82 postmenopausal women. Using the derived structural parameters, patients with and without vertebral fractures could be differentiated significantly better compared to BMD calculated by dual-energy X-ray absorptiometric measurements.

To our knowledge, so far, no study has yet analyzed trabecular bone *in vivo* scans of the lumbar spine or the hip, where significantly more ST is present compared to the thoracic spine. The hip especially is a site of major interest in osteoporosis as fractures here have the most severe health consequences for the patient [27, 28]. This study collected first experience for potential *in vivo* MDCT trabecular bone imaging at the femoral head. Other skeletal sites, like the femoral neck, the trochanteric region, and the spine, still have to be investigated. Stauber and Muller [31] revealed major differences in local bone morphology and isotropy among different skeletal sites. However, as the femoral head shows a high anisotropy and a high BMD, it may be one of the most challenging skeletal sites to image

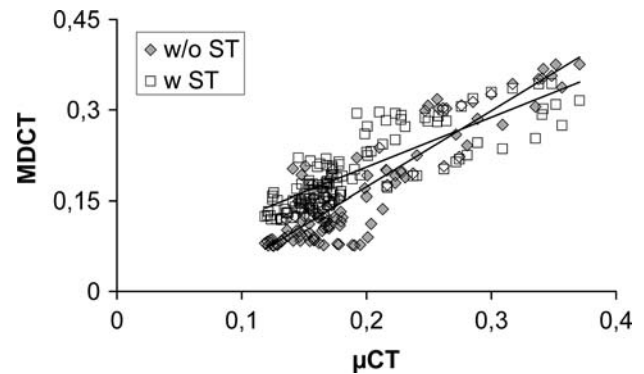


**Fig. 4** Regression curves of bone fraction (BV/TV) for MDCT w ST and w/o ST vs.  $\mu$ CT

trabecular structure *in vivo*. On the other hand, the femoral head proved to be the best-suited site to predict femur strength using trabecular structural parameters [8].

In contrast to magnetic resonance imaging, MDCT can be applied with less operator interaction and is thus well suited for standardized and automated evaluation of trabecular and cortical bone. In particular the thresholding can better be standardized as a calibration is possible with specific phantoms. In recent MDCT studies, the threshold was optimized visually just for the specific study. With this approach, the range of structural patterns within one study could be visualized best but a comparison between different studies was not possible. Future research is needed to provide a consistent and objective thresholding technique for different MDCT studies.

Krug et al. [32] recently tried to visualize trabecular structure of the hip using magnetic resonance (MR). Despite the use of a 3.0T MR scanner, SNR was still a major problem and only a relatively low spatial resolution could be achieved. The data of this study suggest that MDCT is able to provide trabecular bone structure information: the correlation between  $\mu$ CT and MDCT was high for three out of four structural parameters in the scans w and w/o surrounding ST equivalent. The parameters Tb.N and Tb.Th showed no significant difference between the scans w and w/o ST, concerning the correlation with  $\mu$ CT. In case of BV/TV, the limitations introduced by the ST were visible: the correlation with  $\mu$ CT decreased, while the residual errors increased significantly. The range of the derived values for BV/TV was smaller in the scans w ST, as demonstrated in Figure 4 by the reduced slope in the regression curve. The correlations found in this study, both w and w/o ST, were in the same range compared to other studies, performed without surrounding ST: Phan et al. [33] found correlations between  $\mu$ CT-derived and MR-derived trabecular structural parameters of up to 0.87 for app. BV/TV and of up to 0.79 for app. Tb.N. Bauer et al. [5] compared  $\mu$ CT and MDCT data sets of the spine in 20 bone speci-

mens and found correlations of up to 0.89 for app. BV/TV and of up to 0.91 for app. Tb.N. The parameter app. Tb.Th did not show significant correlations between MDCT and  $\mu$ CT. This was not unexpected as the average trabecular thickness is below the used voxel size of MDCT. Other studies had similar results [5, 34].

Due to the experimental setup of this study, some limitations may have to be considered. First, some air was present within the phantom and only a small bone volume was analyzed; thus, the setup may not represent a truly *in vivo*-like situation. However, the hip shows a high anisotropy; as we wanted to minimize averaging effects of the structural parameters within one analyzed volume, the compared regions had to be small: 126 matching regions seemed to be sufficient for this purpose. Second, only one skeletal site was analyzed. Although the femoral head seems to be the most challenging site for determination of trabecular structural parameters *in vivo*, the results of this study may not be applicable for different parts of the proximal femur and other skeletal sites. The samples were obtained from patients with osteoarthritis; thus, osteoporotic bone was not analyzed specifically. In our experience, apparent structural parameters can be calculated more accurately in osteoporotic bone as trabeculae are less dense and, thus, partial volume effects are less pronounced. Third, only visual image registration was applied and robust image registration is required when analyzing trabecular bone at the whole proximal femur *in vivo*. Automated software for this purpose is not yet available for *in vivo* scans, but this work is currently in progress at our institution.

In conclusion, structural analysis of the proximal femur in an *in vivo*-like setting is limited by scattering artifacts that substantially compromise image quality and result in an eightfold decrease in SNR and CNR. However, the major characteristics of the trabecular network can still be appreciated and quantified. MDCT-based techniques therefore have the potential to visualize and quantify trabecular structure *in vivo* at skeletal sites within the torso such as the proximal femur.

## References

- Adachi JD, Loannidis G, Berger C, Joseph L, Papaioannou A, Pickard L, Papadimitropoulos EA, Hopman W, Poliquin S, Prior JC, Hanley DA, Olszynski WP, Anastassiades T, Brown JP, Murray T, Jackson SA, Tenenhouse A (2001) The influence of osteoporotic fractures on health-related quality of life in community-dwelling men and women across Canada. *Osteoporos Int* 12:903–908
- Burge R, Dawson-Hughes B, Solomon DH, Wong JB, King A, Tosteson A (2007) Incidence and economic burden of osteoporosis-related fractures in the United States, 2005–2025. *J Bone Miner Res* 22:465–475
- Thomsen JS, Laib A, Koller B, Prohaska S, Mosekilde L, Gowin W (2005) Stereological measures of trabecular bone structure: comparison of 3D micro computed tomography with 2D histological sections in human proximal tibial bone biopsies. *J Microsc* 218(pt 2):171–179
- Link TM, Vieth V, Stehling C, Lotter A, Beer A, Newitt D, Majumdar S (2003) High-resolution MRI vs multislice spiral CT: which technique depicts the trabecular bone structure best? *Eur Radiol* 13:663–671
- Bauer JS, Issever AS, Fischbeck M, Burghardt A, Eckstein F, Rummeny EJ, Majumdar S, Link TM (2004) Multislice-CT for structure analysis of trabecular bone - a comparison with micro-CT and biomechanical strength [in German]. *Rofo* 176:709–718
- Ito M, Ikeda K, Nishiguchi M, Shindo H, Uetani M, Hosoi T, Orimo H (2005) Multi-detector row CT imaging of vertebral microstructure for evaluation of fracture risk. *J Bone Miner Res* 20:1828–1836
- Patel PV, Prevrhal S, Bauer JS, Phan C, Eckstein F, Lochmuller EM, Majumdar S, Link TM (2005) Trabecular bone structure obtained from multislice spiral computed tomography of the calcaneus predicts osteoporotic vertebral deformities. *J Comput Assist Tomogr* 29:246–253
- Bauer JS, Kohlmann S, Eckstein F, Mueller D, Lochmuller EM, Link TM (2006) Structural analysis of trabecular bone of the proximal femur using multislice computed tomography: a comparison with dual X-ray absorptiometry for predicting biomechanical strength *in vitro*. *Calcif Tissue Int* 78:78–89
- Ruegsegger P, Koller B, Muller R (1996) A microtomographic system for the nondestructive evaluation of bone architecture. *Calcif Tissue Int* 58:24–29
- Muller R, Van Campenhout H, Van Damme B, Van Der Perre G, Dequeker J, Hildebrand T, Ruegsegger P (1998) Morphometric analysis of human bone biopsies: a quantitative structural comparison of histological sections and micro-computed tomography. *Bone* 23:59–66
- Issever AS, Vieth V, Lotter A, Meier N, Laib A, Newitt D, Majumdar S, Link TM (2002) Local differences in the trabecular bone structure of the proximal femur depicted with high-spatial-resolution MR imaging and multisection CT. *Acad Radiol* 9:1395–1406
- Parfitt AM, Drezner MK, Glorieux FH, Kanis JA, Malluche H, Meunier PJ, Ott SM, Recker RR (1987) Bone histomorphometry: standardization of nomenclature, symbols, and units. Report of the ASBMR Histomorphometry Nomenclature Committee. *J Bone Miner Res* 2:595–610
- Harrigan TP, Mann RW (1984) Characterization of microstructural anisotropy in orthotropic materials using a 2nd rank tensor. *J Materials Sci* 19:761–767
- Durand EP, Ruegsegger P (1991) Cancellous bone structure: analysis of high-resolution CT images with the run-length method. *J Comput Assist Tomogr* 15:133–139
- Link TM, Majumdar S, Augat P, Lin JC, Newitt D, Lu Y, Lane NE, Genant HK (1998) *In vivo* high resolution MRI of the calcaneus: differences in trabecular structure in osteoporosis patients. *J Bone Miner Res* 13:1175–1182
- Majumdar S, Newitt D, Mathur A, Osman D, Gies A, Chiu E, Lotz J, Kinney J, Genant H (1996) Magnetic resonance imaging of trabecular bone structure in the distal radius: relationship with X-ray tomographic microscopy and biomechanics. *Osteoporos Int* 6:376–385
- Flohr T, Stierstorfer K, Raupach R, Ulzheimer S, Bruder H (2004) Performance evaluation of a 64-slice CT system with z-flying focal spot. *Rofo* 176:1803–1810
- Ohnesorge B, Flohr T, Schaller S, Klingenberg-Regn K, Becker C, Schopf UJ, Bruning R, Reiser MF (1999) The technical bases and uses of multi-slice CT [in German]. *Radiologe* 39:923–931

19. Prevrhal S (1993) Ein neuer Algorithmus in der computertomographischen Bildrekonstruktion [PhD diss]. Institute of Applied and Technical Physics, University of Vienna
20. Siewerdsen JH, Daly MJ, Bakhtiar B, Moseley DJ, Richard S, Keller H, Jaffray DA (2006) A simple, direct method for X-ray scatter estimation and correction in digital radiography and cone-beam CT. *Med Phys* 33:187–197
21. Prevrhal S, Engelke K, Kalender WA (1999) Accuracy limits for the determination of cortical width and density: the influence of object size and CT imaging parameters. *Phys Med Biol* 44:751–764
22. Gupta R, Grasruck M, Suess C, Bartling SH, Schmidt B, Stierstorfer K, Popescu S, Brady T, Flohr T (2006) Ultra-high resolution flat-panel volume CT: fundamental principles, design architecture, and system characterization. *Eur Radiol* 16:1191–1205
23. Gordon CL, Lang TF, Augat P, Genant HK (1998) Image-based assessment of spinal trabecular bone structure from high-resolution CT images. *Osteoporos Int* 8:317–325
24. Cortet B, Dubois P, Boutry N, Palos G, Cotten A, Marchandise X (2002) Computed tomography image analysis of the calcaneus in male osteoporosis. *Osteoporos Int* 13:33–41
25. Abrahamsen B, Hansen TB, Jensen LB, Hermann AP, Eiken P (1997) Site of osteodensitometry in perimenopausal women: correlation and limits of agreement between anatomic regions. *J Bone Miner Res* 12:1471–1479
26. Eckstein F, Lochmuller EM, Lill CA, Kuhn V, Schneider E, Dellling G, Muller R (2002) Bone strength at clinically relevant sites displays substantial heterogeneity and is best predicted from site-specific bone densitometry. *J Bone Miner Res* 17:162–171
27. Looker AC, Orwoll ES, Johnston CC Jr, Lindsay RL, Wahner HW, Dunn WL, Calvo MS, Harris TB, Heyse SP (1997) Prevalence of low femoral bone density in older U.S. adults from NHANES III. *J Bone Miner Res* 12:1761–1768
28. Ray NF, Chan JK, Thamer M, Melton LJ III (1997) Medical expenditures for the treatment of osteoporotic fractures in the United States in 1995: report from the National Osteoporosis Foundation. *J Bone Miner Res* 12:24–35
29. Link TM, Majumdar S, Lin JC, Augat P, Gould RG, Newitt D, Ouyang X, Lang TF, Mathur A, Genant HK (1998) Assessment of trabecular structure using high resolution CT images and texture analysis. *J Comput Assist Tomogr* 22:15–24
30. Link TM, Majumdar S, Lin JC, Newitt D, Augat P, Ouyang X, Mathur A, Genant HK (1998) A comparative study of trabecular bone properties in the spine and femur using high resolution MRI and CT. *J Bone Miner Res* 13:122–132
31. Stauber M, Muller R (2006) Volumetric spatial decomposition of trabecular bone into rods and plates – a new method for local bone morphometry. *Bone* 38:475–484
32. Krug R, Banerjee S, Han ET, Newitt DC, Link TM, Majumdar S (2005) Feasibility of in vivo structural analysis of high-resolution magnetic resonance images of the proximal femur. *Osteoporos Int* 16:1307–1314
33. Phan CM, Matsuura M, Bauer JS, Dunn TC, Newitt D, Lochmuller EM, Eckstein F, Majumdar S, Link TM (2006) Trabecular bone structure of the calcaneus: comparison of MR imaging at 3.0 and 1.5 T with micro-CT as the standard of reference. *Radiology* 239:488–496
34. Kothari M, Keaveny T, Lin J, Newitt D, Genant H, Majumdar S (1998) Impact of spatial resolution on the prediction of trabecular architecture parameters. *Bone* 22:437–443